Brain Stimulation 18 (2025) 1939–1951

Contents lists available at ScienceDirect

Brain Stimulation

journal homepage: www.journals.elsevier.com/brain-stimulation

A multifunctional theranostic ultrasound platform for remote magnetogenetics and expanded blood-brain barrier opening

Alec J. Batts [a,*], Fotios N. Tsitsos [a], Jeannette Ingabire [b], Guillaume Duret [c], Samantha L. Gorman [a], Deny Tsakri [a], Rebecca L. Noel [a], Robin Ji [a], Nancy Kwon [a], Quoc-Khanh Pham [c], Linlin Zhang [c], Gang Bao [c], Jacob T. Robinson [c,d,e], Elisa E. Konofagou [a,f,g,**]

[a] Dept. of Biomedical Engineering, Columbia University, New York, NY, USA
[b] Systems, Synthetic and Physical Biology PhD Program, Rice University, Houston, TX, USA
[c] Dept. of Bioengineering, Rice University, Houston, TX, USA
[d] Dept. of Electrical and Computer Engineering, Rice University, Houston, TX, USA
[e] Dept. of Neuroscience, Baylor College of Medicine, Houston, TX, USA
[f] Dept. of Radiology, Columbia University, New York, NY, USA
[g] Dept. of Neurosurgery, Columbia University, New York, NY, USA

A B S T R A C T

Introduction: Brain stimulation techniques are critical for unraveling the innerworkings of complex neuronal pathways governing both normal physiological function and pathologic states in neurological disorders. Focused ultrasound (FUS) is an emerging technique poised to significantly alter central nervous system (CNS) drug delivery and neuroscience research through non-invasive means. Magnetogenetics is a brain stimulation technique which may benefit from FUS technology in that alternating magnetic fields (AMF), like FUS, can pass through the skull without requiring surgery.

Methodology: Magnetogenetics involves the deposition of superparamagnetic iron-oxide nanoparticles (SPIONs) and overexpression of thermoreceptor transmembrane proteins (e.g. TRPV1 and TRPA1) in the brain. When an external AMF is applied, SPIONs generate local heating, which can activate thermoreceptors, depolarize the cell membrane and trigger action potentials in neurons. Monitoring neuronal activation by a magnetogenetics approach can be facilitated by the co-expression of genetically-encoded voltage indicators (GEVI), which enable fluorescence-based detection of membrane depolarization. However, traditional surgical methods used to introduce these components into the brain are invasive and highly focal, precluding investigation of brain-wide neuronal pathways.

Results: Here, we demonstrate that our recently developed, flexible configuration for FUS therapy and ultrasound imaging, called theranostic ultrasound (ThUS), can transiently open the blood-brain barrier (BBB) and facilitate the non-invasive delivery of SPION and viral vectors encoding thermoreceptors and GEVI, to enable remote magnetogenetic modulation. We also report significant advances in ThUS pulse sequence design, where we developed a novel multi-target opening volume expansion (MOVE) pulse sequence to maximize BBB opening volume within a single ThUS treatment. ThUS MOVE yielded increased gene delivery commensurate with the number of targeted focal zones and achieved brain-wide expression of GEVI.

Conclusion: The results presented herein not only demonstrate the feasibility for ThUS to facilitate a non-invasive brain stimulation approach, but also showcase a method for eliciting larger volumes of BBB opening within a single sonication which could dramatically improve gene delivery procedures for both preclinical research and therapeutic purposes in the future.

1. Introduction

Transcranial focused ultrasound (FUS) in conjunction with systemically-administered acoustic contrast agents including microbubbles has been repeatedly demonstrated to non-invasively elicit transient, safe, and reversible opening of the blood-brain barrier, conferring a host of therapeutic bioeffects [1–6]. These include immunotherapeutic benefits and memory improvement in neurodegenerative disorders including Alzheimer's disease (AD) [7–14], targeted delivery of chemo- or immunotherapies to brain tumors [15–19] and gene delivery for movement disorders such as Parkinson's disease (PD) [8,20–24] to name a few. The majority of FUS studies to date have employed spherically-focused FUS transducers, where ultrasound energy is concentrated at a highly precise focal volume which is fixed in

* Corresponding author.
** Corresponding author. Dept. of Biomedical Engineering, Columbia University, New York, NY, USA.
E-mail addresses: ajb2305@columbia.edu (A.J. Batts), ek2191@columbia.edu (E.E. Konofagou).

https://doi.org/10.1016/j.brs.2025.10.006
Received 17 July 2025; Received in revised form 26 September 2025; Accepted 6 October 2025
Available online 8 October 2025

design in the case of FUS transducers made up of only a single element. Clinically speaking, most FUS therapy is conducted under guidance by magnetic resonance imaging (MRI), comprising a modality called Magnetic Resonance-guided Focused Ultrasound (MRgFUS). FUS transducers within these MRgFUS systems are also spherically-focused, exhibiting a highly precise focal volume. However, unlike single-element transducers, they contain multiple elements which aid in correcting phase differences attributed to ultrasound penetration through the human skull [25]. MRgFUS systems are generally costly, in that a dedicated MRI scanner is required for intraoperative guidance and monitoring of FUS therapy. Our group has developed a novel technique for transcranial therapeutic ultrasound, which addresses some of the limitations posed by MRgFUS systems, by combining ultrasound imaging and FUS therapy within the same transducer [3,4,26–29]. This "theranostic" approach, referred to herein as theranostic ultrasound (ThUS), utilizes a repurposed linear diagnostic phased array transducer operated with conventional diagnostic ultrasound scanner hardware, making transcranial FUS therapy more portable and accessible. Thanks to the imaging array configuration, we can monitor and image microbubble activity in response to ThUS during the treatment. Such activity is associated with BBB opening volume and transgene expression after gene delivery to the brain [3]. Additionally, although clinical MRgFUS systems are also capable of electronic beam steering, their tightly focused beams require prolonged sonication durations to achieve large BBB opening volumes due to their high spatial precision. In contrast, the inherently less focused nature of the ThUS transducer, owing to its linear phased-array design, allows for a broader BBB opening per sonication. When combined with electronic beam steering and rapid target-switching, this enables more efficient sonication of larger brain regions in substantially less time.

Innovations in focused ultrasound (FUS) have primarily aimed to establish alternative clinical treatments for neurological disorders, but its non-invasive and targeted drug delivery capabilities also make it a valuable tool for preclinical neuroscience research. Many brain stimulation techniques, including optogenetics and chemogenetics, require the invasive delivery of transgenes to neurons, often through intraparenchymal injection of viral vectors. Optogenetics, in particular, is further limited by the poor penetrance of light through the skull and brain tissue, making it challenging to target deep or widespread neuronal populations [30]. Magnetogenetics offers a promising alternative by combining gene-based expression of thermosensitive ion channels with magnetic actuators—typically superparamagnetic iron oxide nanoparticles (SPIONs)—which locally heat in response to alternating magnetic fields (AMFs) to stimulate neuronal activity [31]. This AMF-based approach enables wireless activation of deep brain targets and large-scale neural networks, with the added potential for multiplexed control using nanoparticles tuned to distinct AMF frequencies. To enable magnetogenetic neuromodulation, however, both transgenes and SPIONs must still be delivered to specific brain regions, highlighting the need for less invasive delivery strategies such as ThUS.

Relative to optogenetics, magnetogenetics traditionally suffers from latency between stimulus and response governed by the time required for nanoparticle to reach a temperature threshold specific to cellular thermoreceptors. Prior magnetogenetics studies have confirmed AMF-mediated heating of ferromagnetic nanoparticles to activate transmembrane Transient Receptor Potential Vanilloid 1 (TRPV1), enabling remote stimulation of neurons [32,33]. In more recent magnetogenetics studies, Transient Receptor Potential Ankyrin 1 (TRPA1) was shown to elicit faster response times relative to TRPV1 [31]. While TRPV1 activates after temperature reaches a threshold, TRPA1-A is postulated to respond to the rate of heating [34]. This rate-sensitivity coupled to a rapid SPION-mediated temperature rise, enabled sub-second neuronal stimulation in *drosophila* [31].

While SPION coupled with TRPA1-A enables neuromodulation, the additional expression of cellular activity indicators can help monitor the associated neuron activity in vivo. Engineering of genetically-encoded voltage indicators (GEVI) has facilitated recording of individual neurons through changes in fluorescence intensity as a response to transmembrane voltage [35,36]. Next generation GEVI, including pAce and pAceR, can be used to monitor dynamics of multiple populations of neurons in vivo [37], which when used together with AMF, SPION and TRPA1-mediated neuromodulation, provides a readout for remote magnetogenetics stimulation with both high spatial and temporal resolution.

The genes for the aforementioned GEVI and TRP proteins are typically delivered using adeno-associated viruses (AAV), which are considered a premier viral gene delivery vehicle due to their innate targeting advantages conferred by capsid tropism, durable transgene expression on the order of 6 months to 2 years [38], and low immunogenicity. However, AAV vectors are typically administered via intraparenchymal injection, which can lead to tissue damage and limit the spatial extent of gene delivery [39]. Given that ThUS induces a level and distribution of AAV transduction in brain regions modulated by the ThUS parameters used [3], we hypothesize that ThUS may be able to noninvasively deliver both magnetic nanoparticles and AAV particles to establish a fully remote, and non-surgical magnetogenetics approach in vivo.

In this preclinical study, our primary goal was to demonstrate the utility of a novel FUS pulse sequence in a neuroscience setting, specifically for noninvasively delivering all the key components required for magnetogenetics (GEVI, thermoreceptors, and magnetic nanoparticles) to the same brain region. The novelty of this work lies in several firsts: no prior studies have demonstrated GEVI delivery via FUS, TRPA1 expression in neurons following FUS, or metallic nanoparticle delivery with FUS. Here, we validate the ThUS-facilitated delivery and colocalization of SPION, TRPA1, and GEVI, as a step toward synergistic and remote magnetogenetics in vivo. Furthermore, we expand upon the ThUS parameter space and pulse sequence design to achieve increased gene expression across a larger volume of BBB opening using the novel multi-target opening volume expansion (MOVE) pulse sequence facilitated by the ThUS multielement phased array platform. These results not only highlight both the advantages and limitations of ThUS for brain stimulation via magnetogenetics but also underscore its flexibility for gene delivery in broader therapeutic applications.

2. Materials and methods

2.1. Animals and study overview

All studies involving animals were conducted in accordance with the Columbia University Institutional Animal Care and Use Committee (IACUC). A total of 21 male C57BL/6J wild-type mice (Jackson Labs) ranging from 8 to 10 weeks of age were used across five main experimental protocols. The experiments presented herein were designed to achieve two objectives: i) to determine feasibility for non-invasive delivery and colocalization of exogenous components for brain stimulation using magnetogenetics (Fig. 1), and ii) to design a pulse sequence to enlarge volumes of BBB opening and viral transduction during a single sonication (Fig. 2). For characterization of SPION delivery based on particle diameter, 7 mice received ThUS-mediated delivery of SPIONs alone using a single ThUS focus targeted to the right visual cortex (n = 3 for 15 nm, n = 2 for 17 nm, n = 2 for 19 nm SPIONs). To assess combined delivery of magnetogenetic components, 3 mice received co-delivery of SPIONs with AAV9-CaMKII-pACE, and 1 mouse received AAV9-CaMKII-pTRPA1. For evaluation of expanded BBB opening pulse sequences, 6 mice were treated with ThUS MOVE variation 1 comparing single-spot versus 3-spot targeting (n = 3 receiving AAV9-hSyn-GFP, n = 3 receiving ThUS only without AAV). Finally, to investigate the effect of burst length on whole-brain delivery, 4 mice received AAV9-CaMKII-pACE with ThUS MOVE variation 2 using 6-spot targeting (n = 2 for 100 pulses per burst, n = 2 for 600 pulses per burst).

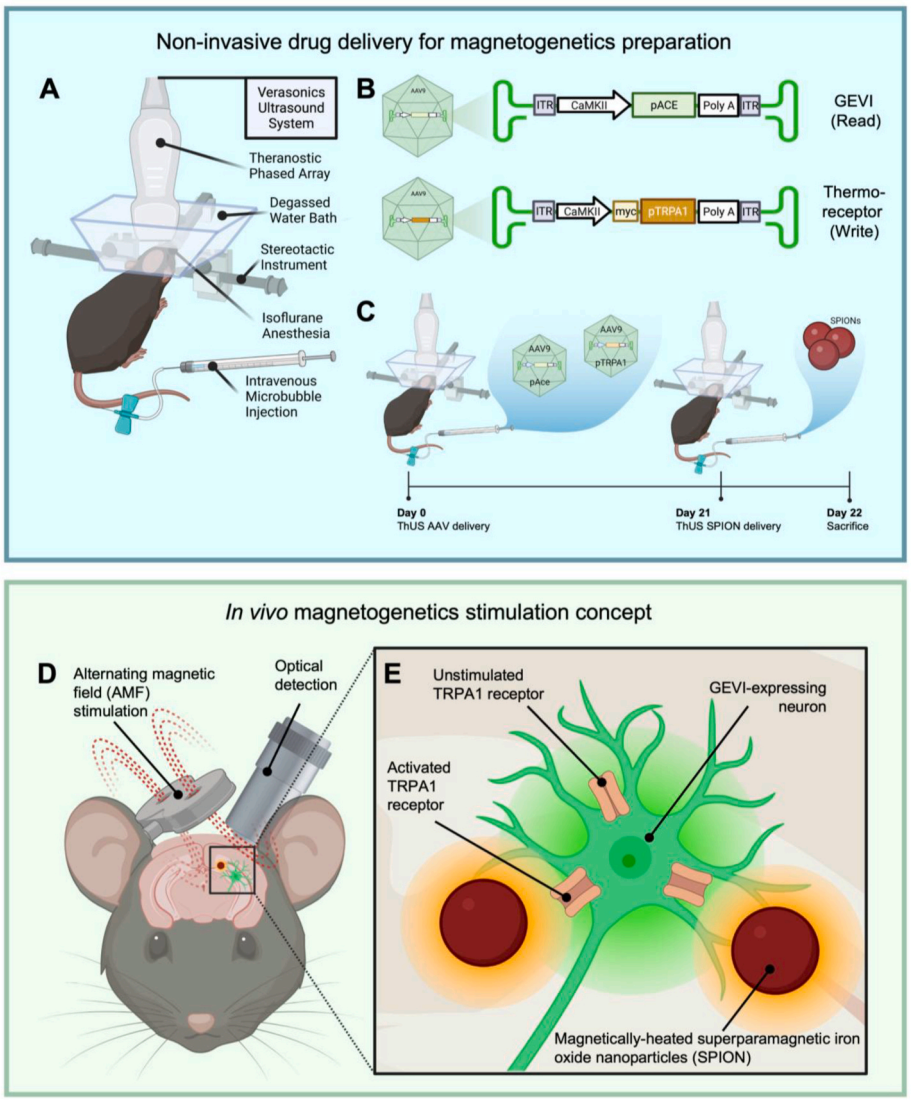

Fig. 1. ThUS-mediated drug delivery for non-invasive magnetogenetics. A) Experimental apparatus for targeted molecular delivery with ThUS. **B)** Diagram of AAV constructs used for recording (GEVI), and modulation (thermoreceptors) of neuronal activity. **C)** Timeline for co-delivery of GEVI and TRPA1 with AAV and SPION with two sessions of ThUS. Note that specific animal numbers for each experiment are disclosed in the Animals and Study Overview section of the Materials and Methods section. **D)** Magnetogenetics platform consisting of external transcranial AMF stimulation of deep brain targets coupled with neuronal voltage imaging. **E)** Magnetogenetic stimulation on the tissue level: AMF-induced heating of SPION increases local temperature, activating rate-sensitive TRPA1 ion channels and initiating neuronal depolarization. Expression of GEVI enable intracellular voltage tracking via cellular fluorescence changes.

2.2. Microbubbles (MBs)

House-manufactured polydisperse MBs were synthesized according to our group's previously published protocols [3,4,40,41]. Briefly, 1, 2-distearoyl-sn-glycero-3-phosphocholine (DSPC, Avanti Polar Lipids Inc., Alabaster, AL, USA) and 1,2-distearoyl-sn-glycero-3-phosphoethanolamine-N-[methoxy (polyethylene glycol)-2000] (DSPC-mPEG2000, Avanti Polar Lipids Inc., Alabaster, AL, USA) were dissolved in a solution of 80 % filtered phosphate-buffered saline (PBS), 10 % glycerol, and 10 % propylene glycol at a 9:1 M ratio at room temperature. Lipids were dissolved by submerging the glass vial containing the solution in a sonication bath maintained above 60 °C until complete dissolution of particles. After cooling to room temperature, the resulting solution was aliquoted into individual 3 mL glass vials and stored at 4 °C.

To prepare MBs for injection on the day of sonication, a sequence of five alternating 20 s intervals of air aspiration and perfluorobutane (PFB) gas administration was conducted to replace ambient air in the vial with PFB. The vial was thoroughly mixed for 45 s using a vial shaker (VialMix™, Lantheus Medical Imaging, N. Billerica, MA, USA) which formed the final solution of lipid-shelled MBs.

MB concentration and size distribution were determined using a particle sizer (Multisizer 4e Coulter Counter, Beckman Coulter, Indianapolis, IN, USA), where the appropriate volume for a final microbubble concentration of 8.0×10^8 MB/mL, corresponding to our group's standard microbubble dose for AAV delivery, was mixed with 100 μL of SPION, or AAV injectate before IV injection through the lateral tail vein during sonication with ThUS.

2.3. Superparamagnetic iron-oxide nanoparticles (SPION)

SPIONs were manufactured at Rice University according to previously described protocols [31,42]. SPIONs were first synthesized at 3 nm and grown to three different diameters: 15 nm, 17 nm and 19 nm; the exact size was determined using TEM imaging of bare nanoparticles. SPIONs were conjugated to [1,1-Dioctadecyl-3,3,3, 3-tetramethylindodicarbocyanine] (DiD) dye for visualization with

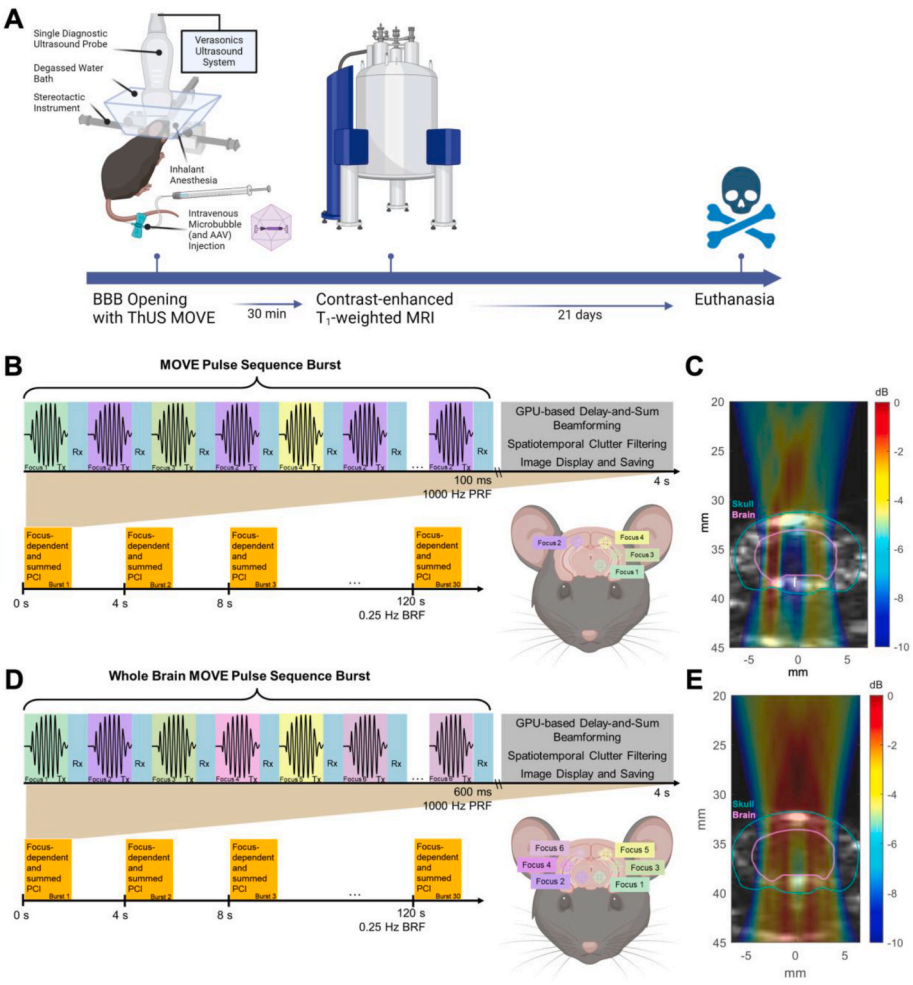

Fig. 2. ThUS MOVE pulse sequence design. A) Experimental timeline and overview. **B)** Diagram of variation 1 of the ThUS MOVE pulse sequence used to evaluate increasing focal areas on BBB opening volume within the same mouse. **C)** Simulated focal region of variation 1 of ThUS MOVE overlaid onto representative pre-sonication B-mode image of the mouse skull. **D)** Diagram of variation 2 of ThUS MOVE used to sonicate the whole mouse brain. **E)** Simulated focal region of variation 2 of ThUS MOVE overlaid onto a representative pre-sonication B-mode image of the mouse skull.

fluorescence microscopy. SPIONs were thoroughly vortexed before dilution in 100 μL of 4 % dextrose for an injected dose of 5–10 mg/kg.

2.4. Adeno-Associated Viruses (AAV)

The AAV9 serotype was used given its previously demonstrated advantage to induce significant brain gene expression after systemic injection and targeted delivery with ThUS [3], and significantly greater transduction efficiency relative to other serotypes when delivered with FUS [43]. AAV9-hSyn-GFP (#50465-AAV9, Addgene, Watertown, MA, USA) was used in development of the ThUS MOVE pulse sequence at a systemic dose of 1.9e11 gc/mouse, while custom AAV9 constructs were used to achieve induction of GEVI and TRPA1 expression in excitatory cortical and hippocampal neurons. AAV9-CaMKII-pAce (University of North Carolina at Chapel Hill (UNC) Vector Core, Chapel Hill, NC, USA) and AAV9-CaMKII-myc-pTRPA1 (Baylor College of Medicine Optogenetics and Viral Vectors Core, Houston, TX, USA) were synthesized and diluted such that a 100 μL volume containing 1.1e11 gc/mouse of each construct was prepared for systemic injection for GEVI and thermoreceptor delivery, respectively (Fig. 1B and C). The difference in AAV dose for development of ThUS MOVE and magnetogenetics implementation is attributed to the low AAV yield for AAV9-CaMKII-myc-pTRPA1 as explained in the discussion section.

2.5. ThUS single-target BBB opening pulse sequence

The single-focus ThUS pulse sequence used for this study consisted of bursts of 100, 10-cycle focused transmits deployed at a pulse repetition frequency (PRF) of 1000 Hz. In between each pulse, the ThUS array received acoustic emissions from oscillating MBs and formed a power cavitation image (PCI) for each burst after a period of GPU-based processing and saving before commencement of the next burst as previously described [3,4,44]. The burst repetition frequency (BRF) for each sonication was 0.33 Hz, yielding approximately 40 frames of PCI for a 2-min sonication duration. This pulse sequence was employed specifically to evaluate SPION delivery to localized brain volumes (Fig. 1C) in contrast to the widespread gene delivery achieved with the novel MOVE sequence as described in the next section.

2.6. ThUS multi-target opening volume expansion (MOVE) pulse sequence

An extension of the ThUS rapid alternating steering angles (RASTA) pulse sequence was developed such that each focused transmit could be deployed at a focal coordinate defined by a steering angle and focal depth. Two variations of the ThUS MOVE pulse sequences were employed to first determine the impact of increased focusing zones on BBB opening volume, and second, determine the feasibility of whole-brain gene delivery with ThUS. For variation 1, a single focal zone

was targeted on one hemisphere of the mouse brain, while 3 focal zones were targeted on the contralateral hemisphere. For each burst, the beam was steered such that odd numbered transmits were deployed to the single target on the left hemisphere, and even numbered transmits were targeted to one of the 3 targets on the right hemisphere (Fig. 2B and C). 6 total transmit pulses encompassed the 4 total targets when following this alternating steering angles paradigm. A fixed number of 100 pulses per burst was used, meaning that more pulses were delivered to the single target on the left hemisphere than each individual target on the right hemisphere by a factor of 3 for each burst. For variation 2, a total of 6 focal zones were targeted to maximize BBB opening within the mouse brain (Fig. 2D and E) with either 100 pulses per burst of 600 pulses per burst. PCI pixel intensity was calculated by summing the intensity across all frames within each burst, then normalizing by the number of pulses per burst to enable direct comparison between conditions while controlling for the different number of frames per burst. This normalization permitted assessment of BBB opening efficiency across burst lengths without artificially inflating PCI values that would result from simply having more frames per burst. In both variations, bursts were repeated for a BRF of 0.25 Hz over a sonication duration of 2 min. Considering the optimal parameter set when weighing both efficacious gene delivery and safety considerations brought about in our previous study [3], for each variation, a fixed 5-cycle pulse length was used.

2.7. ThUS-mediated BBB opening procedure

Transient opening of the BBB for delivery of SPION and AAV was achieved using a ThUS configuration designed for synchronous therapeutic pulses and treatment monitoring via PCI previously developed by our group [3,4]. A P4-1 phased array (ATL, Philips) affixed to a 3D positioner was operated by a research ultrasound system (Vantage 256, Verasonics Inc., Kirkland, WA, USA) to run a custom script for BBB opening and PCI using a center frequency of 1.5 MHz, a fixed peak-negative pressure (PNP) of 1.0 MPa, and ultra-short pulse lengths (USPL) consisting of either 5 or 10 cycles [3] (Fig. 1A). These parameters were evaluated in previous work from our group and have been shown to elicit an acceptable tradeoff between AAV delivery and safety. Mice were anesthetized using a mixture of isoflurane and oxygen, and fixed to a stereotactic instrument (Model 900, David Kopf Instruments, Tujunga, CA, USA) for the duration of the procedure. Fur on the scalp was depilated before placing degassed ultrasound gel and a degassed water bath atop the head for proper acoustic coupling. Targeting of the desired brain region was achieved using B-mode imaging at 2.5 MHz enabled by the P4-1 phased array as previously described in detail [3]. For SPION delivery with ThUS, a single focal region targeting the right visual cortex and hippocampus was sonicated with a beam steering angle of 3.72° and a focal depth of 35 mm as described here [4]. A tail vein catheter was inserted prior to ThUS sonication, where MBs and SPION or AAV were co-injected immediately after initiation of the ThUS pulse sequence. Mice underwent two sessions of ThUS; the first session induced BBB opening for GEVI and TRPA1 delivery, while the second session facilitated SPION deposition within specific brain regions 21 days after the first ThUS session to allow for AAV transduction and gene expression to occur (Fig. 1C). 4 mice underwent a first session with a single focus of ThUS, while 2 mice underwent a first session of ThUS MOVE to evaluate gene expression after brain-wide BBB opening.

Contrast enhanced T_1-weighted MRI were acquired to confirm BBB opening after both ThUS sessions as described in the following section, after which mice were allowed to recover from anesthesia and were survived until euthanasia 24 h after the second ThUS session.

2.8. Magnetic resonance imaging

Contrast-enhanced MRI were acquired 30 min post-ThUS to confirm BBB opening (Fig. 2A). A 0.2 mL IP injection of gadodiamide (Omniscan, GE Healthcare, Princeton NJ, USA) was injected immediately after ThUS before positioning mice in a 30 mm volume coil in the bore of a 9.4 T MRI system (Ascend, Bruker Medical, Billerica, MA, USA) for imaging with a T_1-weighted 2D FLASH sequence (TR: 230 ms, TE: 3.3 ms, Flip angle: 70°, 6 averages, FOV: 25.6 mm × 25.6 mm, Matrix size: 256 × 256, Slice thickness: 0.4 mm, Resolution 0.1 mm × 0.1 mm).

2.9. Animal euthanasia and tissue preparation

Mice were deeply anesthetized before euthanasia by transcardial perfusion with ice cold phosphate buffered saline (PBS). Brains were harvested and soaked in 4 % paraformaldehyde (PFA) for 24 h before cryoprotection in 30 % sucrose in PBS for another 24 h. Brains were coronally cryosectioned into 35-μm-thick slices and mounted onto slides for native pAce and DiD-tagged SPION fluorescence microscopy.

2.10. Microscopy and image analysis

Fluorescence microscopy images were acquired using 10x and 20× dry objectives from either a Leica (DM6 B, Leica Microsystems Inc. Buffalo Grove, IL, USA) or Olympus microscope (BX61, Olympus Corporation, Tokyo, Japan), under DAPI, GFP, and Cy5 filter cubes. Images were exported as TIFF files and were processed using a custom ImageJ script for fluorescence intensity analysis and area quantification which measured the percentage of user-defined regions of interest (ROIs) containing signal above a manually determined threshold following background subtraction. For each brain section, multiple anatomical ROIs were analyzed to determine the spatial distribution of neuronal expression, with results reported as the percent area of each ROI occupied by fluorescent signal. Images of DAB staining of myc-tagged pTRPA1 were acquired on the aforementioned Olympus microscope under brightfield at 20× magnification.

3. Results

3.1. Non-invasive SPION delivery is feasible with ThUS-mediated BBB opening

SPIONs synthesized at two different diameters were non-invasively delivered to a focal volume containing the visual cortex and hippocampus using ThUS in separate mice 24 h before euthanasia. Fluorescence microscopy image analysis of DiD-tagged 15 nm (Fig. 3A) and 19 nm (Fig. 3B) SPIONs in coronal brain sections revealed focal SPION deposition within the sonicated visual cortex and dorsal hippocampus. Image normalization and binarization of fluorescence microscopy images (Fig. 3C and D) revealed no significant differences in the area of DiD fluorescence between SPION size groups (Fig. 3E), or normalized optical density (NOD) of deposited SPIONs (Fig. 3F). At higher magnification, we generally observed increased clustering of SPIONs with increased diameter (Supplementary Fig. 1), suggesting smaller SPIONs may be more homogenously distributed in the targeted brain region after intravenous injection and BBB opening with ThUS. However, evaluation of local temperature elevation after AMF stimulation for each of the SPION formulations to determine which generates sufficient heating for thermosensitive ion channels to activate will be required for further optimization of ThUS-SPION delivery and comprises an important future study to evaluate functional feasibility of heat-sensitive nanoparticles delivered by ThUS-mediated BBB opening.

3.2. Two sessions of ThUS-mediated BBB opening successfully colocalize GEVI and pTRPA1 gene expression with SPIONs

We selected AAV constructs based on the transduction profile of previously evaluated serotype and promoter combinations optimized for targeted brain delivery with ThUS. Two AAV constructs, AAV9-CaMKII-pAce (encapsulating a voltage indicator, GEVI [37]) and AAV9-CaMKII-myc-pTRPA1 (encapsulating a thermoreceptor “neuronal

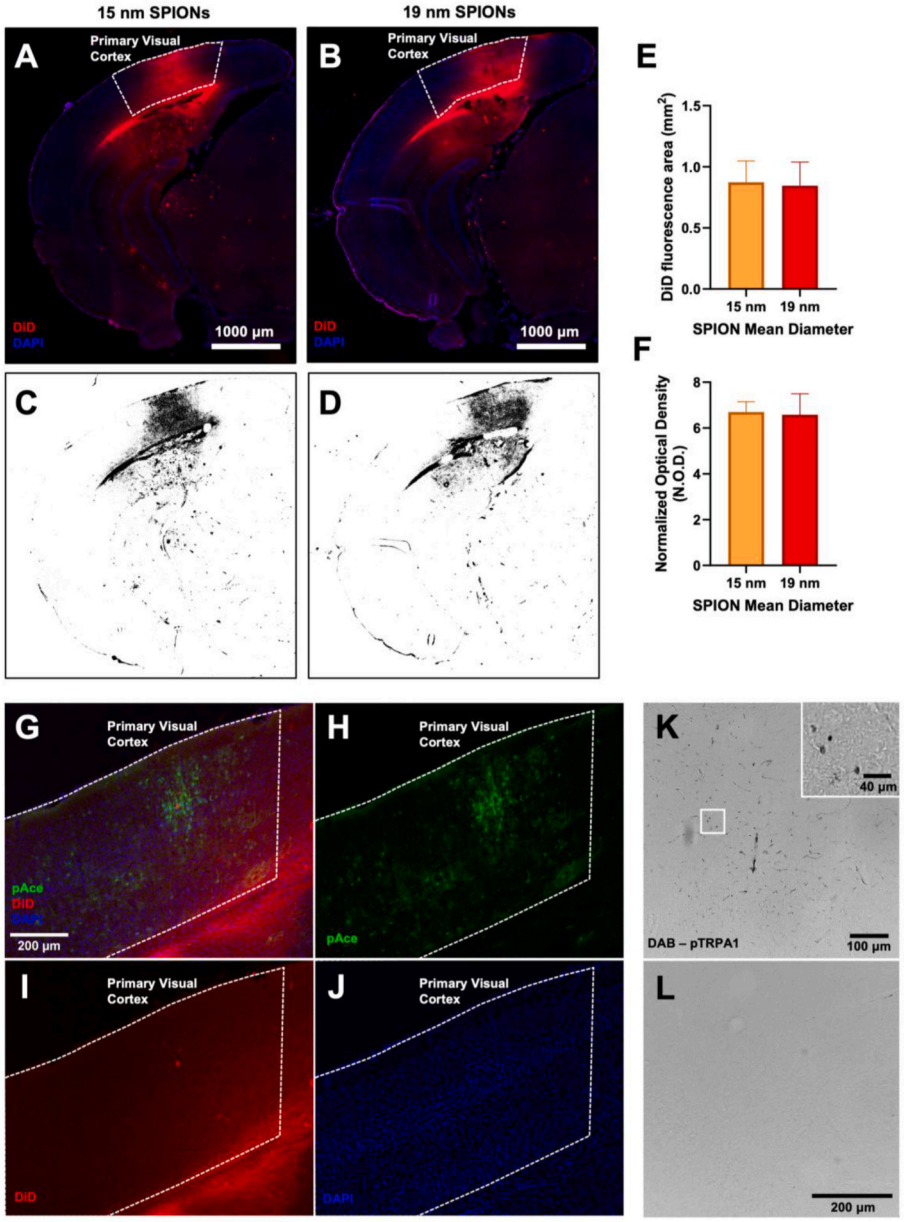

Fig. 3. SPION and AAV delivery with theranostic ultrasound for magnetogenetics. A) Fluorescence microscopy image of representative coronal brain sections depicting DiD fluorescently-tagged 15 nm SPIONs and **B)** 19 nm SPIONs within the sonicated primary visual cortex (dashed line). Binarized images depicting thresholded DiD fluorescence for **C)** 15 nm and **D)** 19 nm SPIONs. Groupwise comparisons between **E)** area and **F)** normalized optical density (NOD) of DiD fluorescence demonstrated no significant differences between SPION diameter. **G)** Merged channel image depicting overlap of SPIONs and pAce GEVI within the sonicated primary visual cortex after two ThUS sessions. Individual channel images of **H)** pAce (GEVI), **I)** DiD (SPIONs), and **J)** DAPI (nuclei). **K)** Brightfield microscopy image depicting DAB staining of myc-tagged pTRPA1 (thermoreceptor) expression in the sonicated visual cortex. Inset corresponds to white rectangular ROI. **L)** Brightfield microscopy image of contralateral visual cortex devoid of pTRPA1 expression.

modulator" [31]) were co-delivered to the visual cortex and hippocampus of mice using the same ThUS parameters employed for SPION delivery. Our goal was to achieve co-expression of both transgenes within the same neuronal population, which would enable simultaneous voltage recording via GEVI and neuronal activity modulation through TRPA1, to facilitate magnetogenetics in vivo. To assess whether SPION could be localized to the same brain region as the resulting transgene expression, a subset of mice received a second ThUS session immediately before euthanasia, targeting SPION delivery to the region where AAV had been introduced 3 weeks earlier. Gene expression was evaluated postmortem with immunohistochemistry and microscopy to confirm successful co-expression and spatial alignment with SPION distribution. Fluorescence microscopy image analysis of coronal brain slices containing pAce expression and SPION deposits exhibited widespread neuronal transduction within the sonicated visual cortex (Fig. 3G–H,J) surrounding regions of concentrated SPIONs (Fig. 3G–J). Colocalization of SPION deposits with pAce expression was also observed in the sonicated dorsal hippocampus (Supplementary Fig. 2), which was also encompassed by the ThUS focal volume, with no detectable fluorescence enhancement in the contralateral brain hemisphere (Supplementary Fig. 2F–I). All mice (n = 3) which underwent two sessions of ThUS demonstrated overlap between pAce expression and DiD fluorescence from SPIONs with an average percent overlap of 43.2 ± 11.9 % (Supplementary Fig. 3).

pTRPA1 expression was targeted to the same populations of neurons as pAce using a construct employing the same CaMKII promoter and

AAV9 serotype. Analysis of bright-field microscopy images confirmed positive DAB signal in the sonicated brain hemisphere indicating pTRPA1 expression in the targeted visual cortex (Fig. 3K). No pTRPA1 expression was detected in the contralateral hemisphere (Fig. 3L). Taken together, these results validate an alternative technique for delivery functional transgenes to the brain, which in turn could enable neuromodulation. Here, the low AAV9-CaMKII-pTRPA1 yield along with constraints related to animal transport prevented testing magnetogenetic neuronal response in these mice. However, we provide the first evidence that ThUS can support noninvasive magnetogenetics by delivering SPIONs and TRP channels to target neurons across the BBB, and can achieve reproducible, localized drug delivery through repeated BBB opening sessions.

3.3. *ThUS MOVE increases BBB opening volume and GEVI delivery commensurate with the number of ThUS focal areas and total ThUS pulses per focal area*

To expand upon the potential viral gene delivery capabilities presented with ThUS in the previous section, the ThUS MOVE sequence was developed in order to achieve a wider distribution of gene expression within the brain. Consistent with our hypothesis, combining electronic axial focusing and lateral beam steering permitted augmentation of the BBB opening volume with a single sonication achieved by rapid alternation of steering angles and focal depths defined by target-specific element-wise phase delays. A total of 6 mice were sonicated with a custom script deploying single-target focused transmits on one hemisphere and three-target focused transmits on the opposite hemisphere at the coordinates specified for variation 1 of ThUS MOVE in the methods section (Fig. 2B). Increasing the number of targeted foci per brain

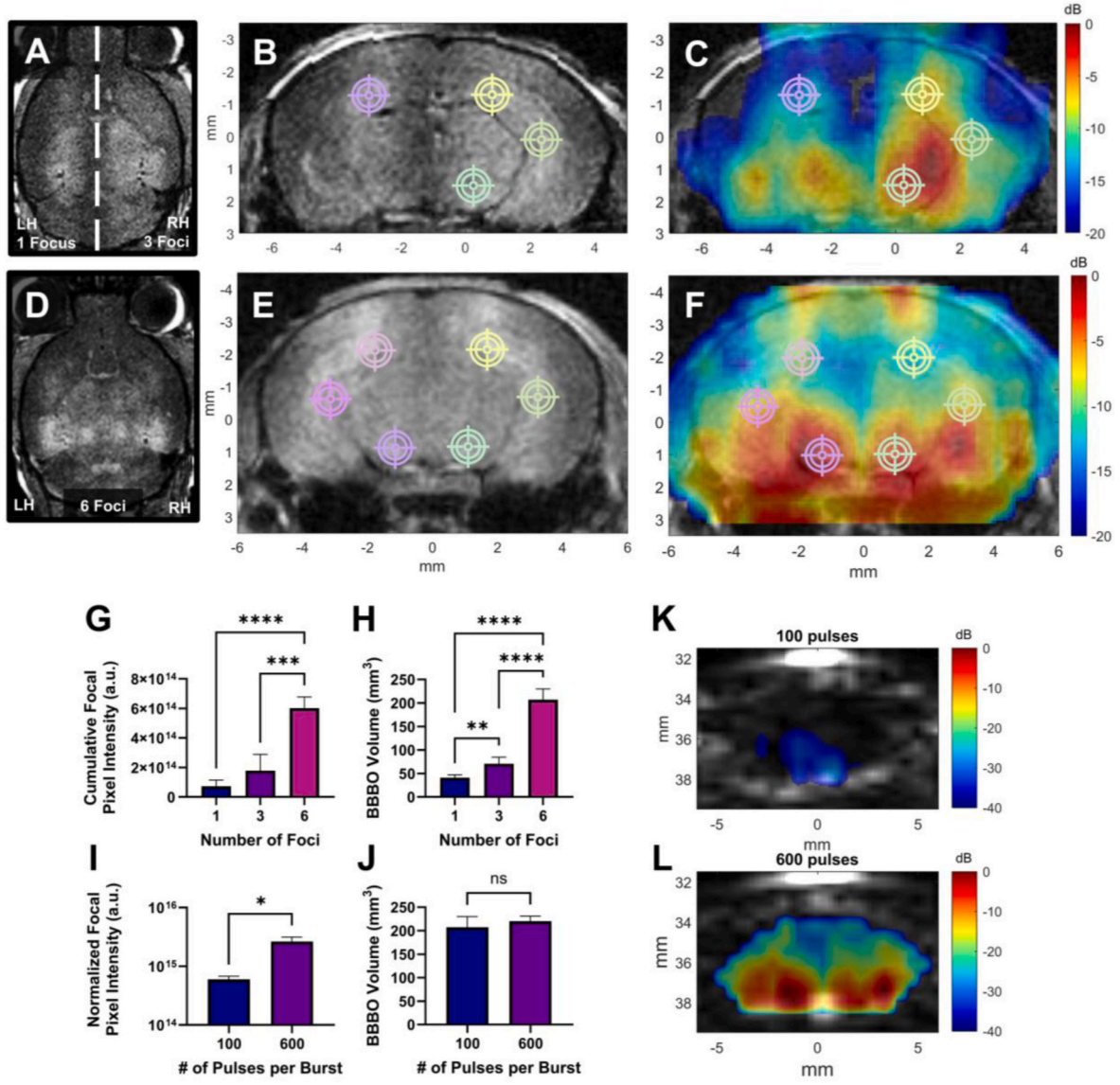

Fig. 4. Enlargement of BBB opening volume with ThUS MOVE. A) Axially-oriented and **B)** coronally-oriented contrast-enhanced T_1-weighted MRI depicting increased BBB opening volume on left hemisphere. **C)** Overlaid PCI and MRI depicting increased cavitation activity on left hemisphere. **D)** Axially oriented and **E)** coronally oriented contrast-enhanced T1-weighted MRI acquired after whole-brain BBB opening with 600 pulses per burst. **F)** Representative PCI depicting cavitation activity during whole-brain BBB opening with 600 pulses per burst. Quantification of significantly increased **G)** PCI pixel intensity and **H)** BBB opening volume with ThUS MOVE. Quantification of **I)** PCI pixel intensity and **J)** BBB opening volume with increasing number of pulses per burst. **K)** Representative PCI overlaid onto B-mode depicting reduced PCI pixel intensity with 100 pulses per burst compared to **L)** with 600 pulses per burst. *$p < 0.05$, **$p < 0.01$, ***$p < 0.001$, ***$p < 0.0001$. Statistical significance in G-H determined by one-way ANOVA with Tukey's multiple comparisons correction, and in I-J by an unpaired *t*-test.

hemisphere yielded a ~2-fold increase in BBB opening volume as confirmed by contrast-enhanced T_1-weighted MRI acquired 20 min post-sonication (Fig. 4A and B). Furthermore, quantification PCI pixel intensity acquired during the sonication revealed significantly increased cavitation activity detected with ThUS, commensurate with the expansion of BBB opening volume (Fig. 4C–G).

In a separate cohort of mice, 6 distinct target locations within the brain were sonicated with variation 2 of the ThUS MOVE sequence to induce BBB opening throughout the entirety of the mouse brain within a single 2-min sonication and bolus microbubble injection (Fig. 2D). Sonication of 6 targets within the brain elicited observable contrast-enhancement on T_1-weighted MRI on both hemispheres extending posterior from the center of the focus through the cerebellum, and anterior from the center of the focal volume through the striatum (Fig. 4D and E), corresponding quantitatively to significant, nearly 2-fold, and 6-fold increases in BBB opening volume relative to the volume of contrast-enhancement elicited by sonication of 3 targets and a single target, respectively (Fig. 4H). Similarly, significant ~3-fold and 8-fold increases in PCI pixel intensity were also observed during whole-brain BBB opening with 6 targets relative to 3 targets and a single target, respectively (Fig. 4G). Additionally, PCI signal intensity within −6 dB of the maximum intensity observed within the brain occupied

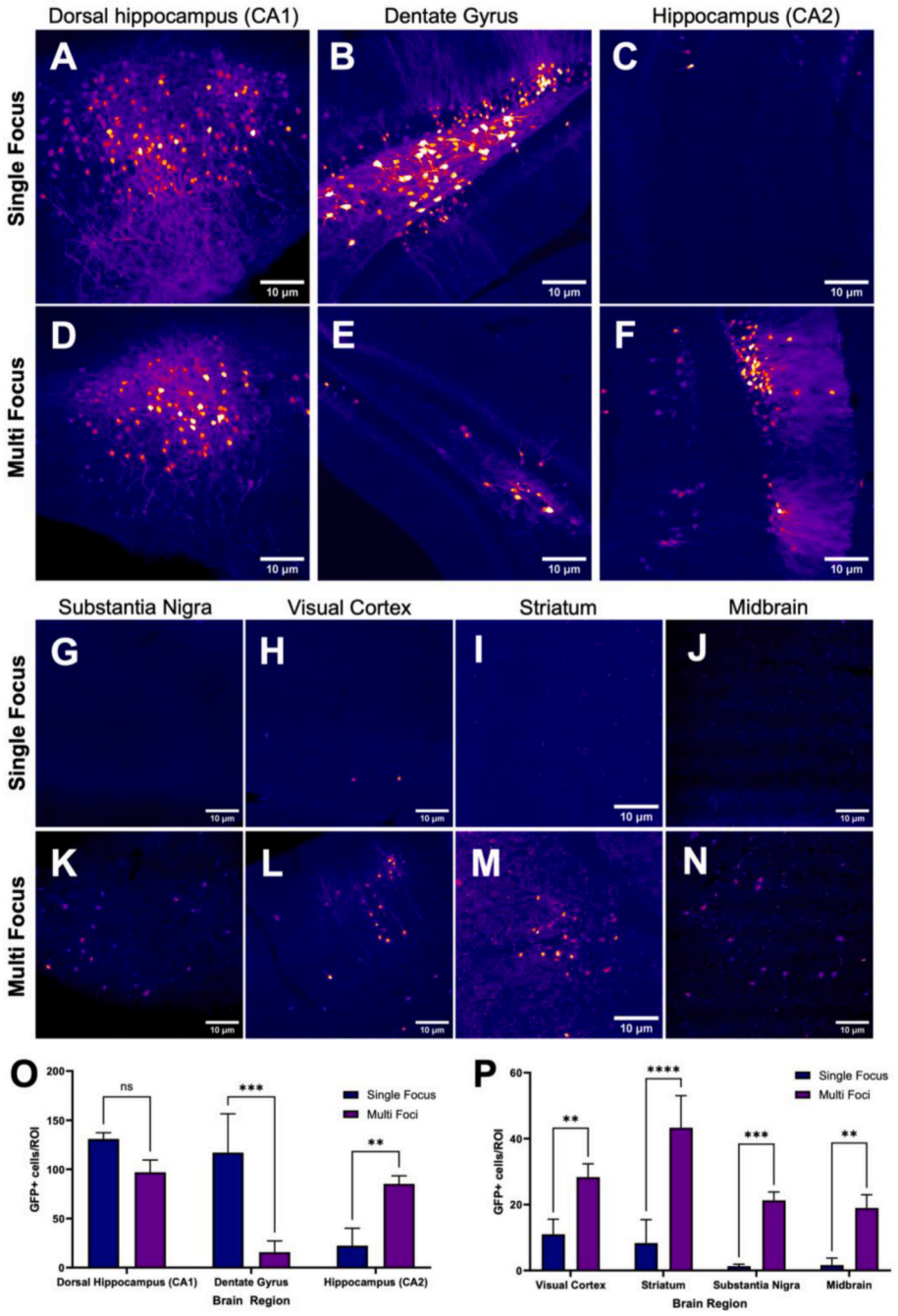

Fig. 5. AAV9-hSyn-GFP delivery with ThUS MOVE. Representative GFP expression along the single focus trajectory in **A)** dorsal hippocampus, **B)** dentate gyrus, and **C)** CA2. Representative GFP expression in **D)** dorsal hippocampus, **E)** dentate gyrus, and **F)** CA2 elicited by BBB opening in 3 targets. Representative GFP expression in **G)** substantia nigra, **H)** visual cortex, **I)** striatum and **J)** midbrain for a single focus, and **K)** substantia nigra, **L)** visual cortex, **M)** striatum, and **N)** midbrain for 3 targets. Quantification **O)** of hippocampal GFP expression, and **P)** non-hippocampal GFP expression. $^{**}p < 0.01$, $^{***}p < 0.001$, $^{****}p < 0.0001$, determined with two-way ANOVA with post-hoc Tukey's multiple comparisons correction.

>86 % of the cross sectional MRI slice at the center of the BBB opening volume, further demonstrating the utility of integrated cavitation mapping to infer the resulting size of BBB opening volume with ThUS (Fig. 4F and G).

While a significant relationship between the number of sonicated focal areas and resulting BBB opening volume and PCI was observed using gadodiamide MR contrast enhancement, the large disparity in molecular weight between gadodiamide and AAV necessitated further investigation to determine whether more focal areas indeed correlated with increased gene expression. To address this, an additional cohort of mice underwent AAV delivery with ThUS MOVE to evaluate whether gene expression patterns aligned with BBB opening expansion observed on MRI. Mice received a bolus injection of AAV9-hSyn-GFP at a dose of 1.9e11 gc/mouse and were survived for 21 days before euthanasia, followed by fluorescence microscopy of sonicated brain sections.

Preliminary quantification of GFP + cells revealed that although brain hemispheres sonicated with 3 targets exhibited more widespread GFP expression, the single-focus condition resulted in significantly higher transgene expression in the dorsal hippocampus and dentate gyrus (Fig. 5A–B, D-E, O). We attribute this to the pulsing paradigm: in the 3-target condition, pulses were distributed among the focal areas, effectively reducing the number of pulses delivered to each individual site compared to the single-focus condition, where all pulses were concentrated in one region. Interestingly, brain hemispheres sonicated with 3 targets exhibited significantly increased GFP expression in the CA2 region of the hippocampus relative to the single-focus condition (Fig. 5C–F, O), likely due to the greater cumulative overlap of the combined −6 dB focal volumes with the CA2 structure (Supplementary Fig. 4). Additionally, in hemispheres sonicated with 3 targets, increased GFP expression was observed in regions outside the primary beam path of the single-focus condition, including the substantia nigra, visual cortex, striatum, and midbrain (Fig. 5G–N, P). These findings underscore

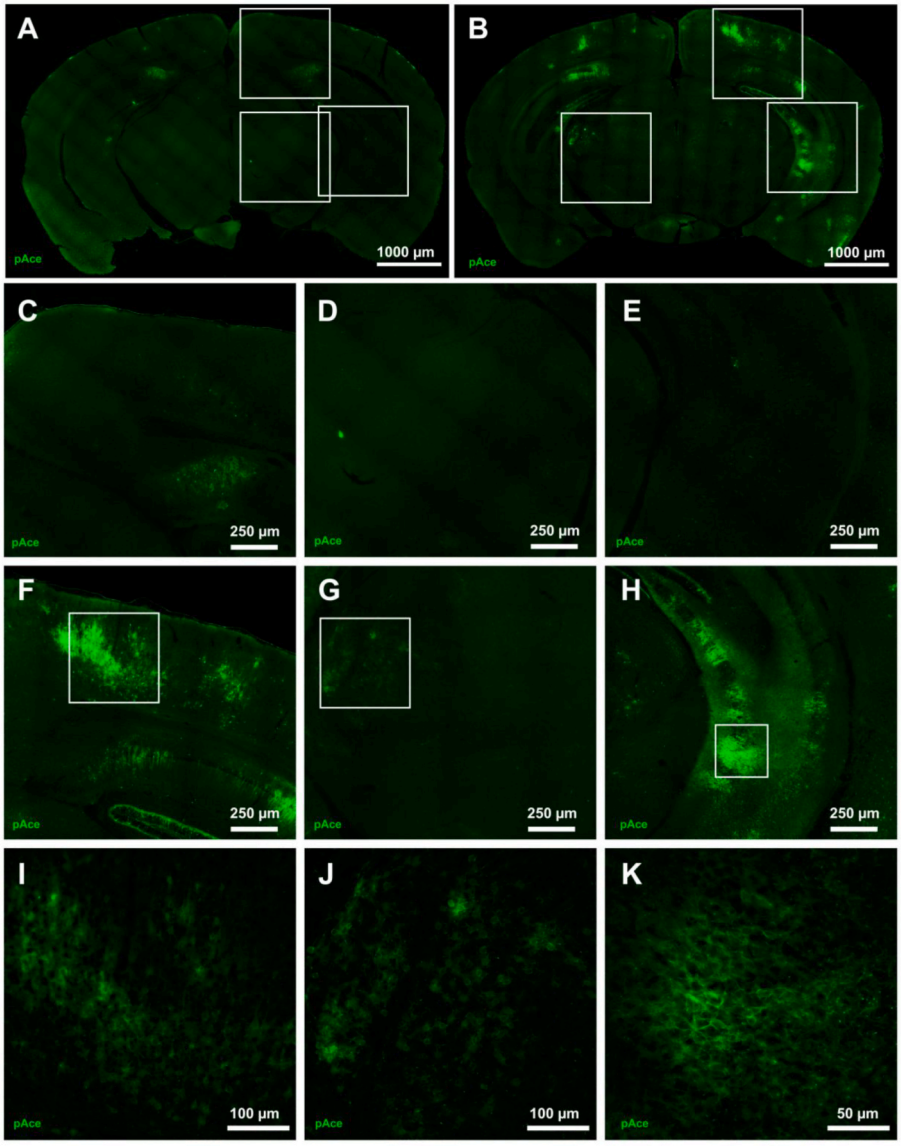

Fig. 6. Increased brain-wide gene expression with optimized ThUS MOVE pulse sequence. A) Representative whole coronal section from a brain sonicated with the ThUS MOVE sequence with 100 pulses per burst depicting the most obvious transduction in the dorsal hippocampus. **B)** Representative whole coronal section from a brain sonicated with a normalized number of pulses per focal area (i.e. 600 pulses), depicting transduction in the cortex, hippocampus, and midbrain. Enlarged images of brain regions sonicated with 100 pulses per burst including the **C)** dorsal hippocampus, **D)** midbrain, and **E)** CA3 hippocampus from rectangular ROIs in A. Enlarged images of brain regions within rectangular ROIs in B sonicated with 600 pulses per burst depicting increased gene transduction with an increase in pulses per burst within the **F)** dorsal hippocampus and visual cortex, **G)** thalamus and midbrain, and **H)** CA3 hippocampus. **I-K)** Enlarged images of rectangular ROIs in F-H.

an important limitation in using MRI contrast enhancement to quantify BBB opening, where broader BBB opening does not necessarily equate to greater transgene expression at a given site. Instead, the spatial distribution of gene expression depends not only on focal volume overlap but also on the pulsing paradigm, which in the multi-target condition effectively reduced the per-site exposure to ThUS pulses, thereby limiting gene expression in individual regions relative to the single-focus condition.

To confirm this, we designed an experiment aimed at exploring the utility of cavitation imaging for AAV delivery, given the constraints of MRI contrast enhancement in precisely reflecting the relationship between BBB opening and resulting gene transduction. By incorporating cavitation-based monitoring, we sought to optimize AAV delivery conditions and revisit the magnetogenetics concept to assess whether brain-wide voltage indicator expression could be achieved non-invasively. To evaluate this, the total number of pulses per burst was increased in proportion to the number of focal areas per sonication, enabling assessment of whole-brain AAV9-CaMKII-pAce delivery. Relative to brains which were sonicated with 6 foci and 100 pulses per burst (Fig. 6A), a 1.8-fold, 14.7-fold and 22.2-fold, increase in pAce expression area was observed in the cortex, hippocampus and midbrain regions, respectively, whereas an overall 4.1-fold increase was observed across whole coronal brain sections (Fig. 6B). While no significant differences in BBB opening volume were detected on contrast-enhanced T_1-weighted MRI (Fig. 4J) in preliminary experiments, likely due to a plateau in gadodiamide contrast accumulation throughout the opening volume when targeting the entire brain, normalized PCI pixel intensity increased over 4-fold with an increase in burst length from 100 to 600 pulses (Fig. 4I–K,L) which agrees with the ~4-fold total increase in gene expression area observed in histology. The 100-pulse burst length yielded gene expression primarily in the dorsal hippocampal area (Fig. 6A–C) with minimal gene expression observed in the midbrain (Fig. 6D) or CA3 region of the hippocampus (Fig. 6E). Conversely, the 600-pulse burst length elicited substantially increased gene expression within the brain (Fig. 6B), most notably within the visual cortex (Fig. 6F–I), thalamus (Fig. 6G–J), and ventral CA3 region of the hippocampus (Fig. 6H–K). These findings highlight the potential of cavitation imaging to enhance AAV delivery by providing real-time feedback on sonication parameters, enabling more precise control over gene transduction. The observed correlation between increased burst length, PCI signal intensity, and greater gene expression suggests that optimizing ultrasound parameters with cavitation monitoring could improve the efficiency and spatial distribution of transgene expression for brain-wide applications of non-invasive viral gene delivery.

4. Discussion

Keeping in mind the overarching aim of this work, we set out to determine whether ThUS-mediated BBB opening could facilitate targeted delivery of molecular machinery required for brain stimulation with magnetogenetics. Given the success of prior magnetogenetics studies to initiate behavioral changes after remote AMF stimulation in conjunction with pTRPA1-A and SPIONs in *Drosophila* [31], we hypothesized that analogous stimulation techniques could elicit similar behavioral responses in mammalian subjects. However, the ability to do so non-invasively remained to be determined. Here, we demonstrated that SPIONs generally exhibited the expected tradeoff between size and deposition area when delivered with ThUS as expected. Notably, larger SPIONs generally elicit increased thermal effects, necessitating further functional studies to determine the relationship between ThUS-facilitated SPION deposition area and heating performance. SPIONs were also sparsely distributed within the ThUS focal volume relative to direct injection-mediated delivery [45], regardless of size, while larger 19 nm SPIONs tended to aggregate. Interestingly, prior studies have demonstrated a reduction in heating performance with increasing aggregate size [46], indicating that smaller SPIONs may be most beneficial for magnetogenetic stimulation given the reduced propensity for aggregation and more uniform distribution observed in this study. Keeping in theme with general observations made throughout this research and prior FUS-mediated BBB opening literature, perhaps a higher systemic dose of SPIONs beyond the 5–10 mg/kg dose prescribed for use in this study would yield more homogeneous SPION deposits throughout the BBB opened area, though short-term and long-term safety of this approach must be evaluated. While the transport kinetics of SPIONs and AAV vary significantly, their diameters are similar. In our previous study, a similar observation was made regarding the effects of dose escalation and homogeneity in brain distribution, where increasing AAV systemic dose yielded more homogeneous gene expression within the ThUS focal volume [3].

In addition to evaluating the initial feasibility of SPION deposition with ultrasound-mediated delivery for the first time, we also extended the applicability of ThUS-mediated AAV delivery for non-invasive, targeted expression of GEVI and pTRPA1 within the same brain regions as SPIONs. GEVI require sufficient expression to visualize many neurons within a given imaging field of view at once, though below a density of expression that precludes visualization of individual cell soma [37]. Prior investigation of the relationship between systemic AAV dose and resulting transgene expression within the brain after ThUS-mediated BBB opening provided insight for the optimal AAV dose required to meet these requirements [3], therefore a systemic dose of 1.1e11 gc/mouse was selected for evaluation in mice. Additionally, we designed a construct to favor GEVI expression in excitatory neurons through the use of the CaMKII promoter [47,48]. With an analogous construct design, AAV9-CaMKII-pTRPA1 was expected to elicit similar patterns of expression as AAV9-CaMKII-pAce, and more specifically, target the same populations of excitatory neurons when co-delivered. While vector synthesis failed to produce enough virus for high-powered animal experiments with systemic administration and targeted delivery with ThUS, pTRPA1 expression was still restricted to ThUS-targeted brain regions where GEVI and SPION were observed, though exact comparisons between GEVI and pTRPA1 co-expression among SPION deposits could not be made. However, given the requirement for all magnetogenetics actuators to be localized within the same brain region, we were indeed able to observe sufficient overlap between GEVI and SPION in several brain regions throughout the ThUS focal volume. While the visual cortex was the main initial target of interest for the experiments conducted in this study for future confirmatory behavioral experiments, the best overlap between GEVI expression and SPION deposits was actually seen in the dorsal hippocampus, and hippocampal-adjacent regions which highly favored gene expression resulting from AAV9 transduction as observed in our previous studies. This indicates potential well-suited applications for ThUS-facilitated magnetogenetics rooted in neuronal circuitry implicated in spatial memory [49–51].

Looking ahead to applications requiring stimulation and recording of many distant brain regions in rodents, or expansion of BBB opening volume for translation of magnetogenetic stimulation techniques in larger animal models utilizing the aforementioned magnetogenetic actuators, we also developed an extension of the ThUS RASTA sequence introduced in our prior study [3]. Here, we sought to enable sonication of more than two anatomically-symmetric targets within the brain to induce larger BBB opening volumes with ThUS. We developed the multi-focal opening volume expansion (MOVE) pulse sequence to i) determine the effect of increased focal zones on BBB opening volume, and ii) evaluate the feasibility of whole-brain BBB opening and AAV delivery. We observed significantly increased BBB opening volume commensurate with trends observed in PCI, beyond its association with modulating BBB opening volume with USPL as described previously, further underscoring the utility of PCI as a reliable treatment monitoring tool for ThUS in vivo. Interestingly, while we observed a general increase in the volume of contrast enhancement in post-ThUS T_1-weighted MRI with increased focal zones, gene expression observed after ThUS-facilitated delivery of 1.9e11 gc/mouse of AAV9-hSyn-GFP

appeared to be highly dependent on the number of pulses delivered to each focal volume, and did not quantitatively correlate with the volume of contrast enhancement calculated from MRI. In other words, the data obtained using variation 1 of ThUS MOVE elucidated the requirement for burst length normalization to ensure equal ThUS exposure across all targeted foci. This hypothesis was tested through experimentation with variation 2 of ThUS MOVE, where a normalized number of 600 pulses per burst, corresponding to 100 pulses per focal zone, achieved significantly greater brain-wide gene expression compared to sonications where 100 pulses were split evenly among all focal zones. Furthermore, the increase in resulting gene expression was supported by a significant increase in PCI pixel intensity even after normalization of the increased number of PCI frames acquired with longer burst lengths, but was not supported by increased BBB opening volume derived from MRI. This observation crucially underscores the utility of PCI to garner increased predictive value of the extent of gene delivery where anatomical MRI fails to do so given the difference in transport capabilities between gadodiamide and AAV.

Beyond these findings, an important consideration for optimizing AAV delivery efficiency is facilitating increased BBB opening volume during a single sonication event. Achieving a greater BBB opening volume in one “shot”, or after a single microbubble bolus injection, minimizes the need for transducer repositioning in the case of single-element transducers that inherently lack electronic beam steering capabilities, thereby reducing experimental complexity, variability in targeting, and inconsistencies related to microbubble injection timing and dosage. The relatively unfocused nature of the ThUS linear phased array geometry also creates a larger focal zone compared to the tightly focused beams of hemispherical multi-element MRgFUS arrays, which were originally designed for precise tissue ablation. While MRgFUS systems offer excellent beam steering capabilities and spatial precision, their small focal volumes require a greater number of sonication points to achieve BBB opening across larger brain regions. The larger focal geometry of ThUS, owing to the design of the diagnostic phased array transducer, allows greater BBB opening volumes per sonication, reducing the total number of targeting points needed and thereby decreasing overall treatment time. This strategy could be advantageous in clinical translation by reducing treatment times and enabling more efficient gene delivery to larger brain structures such as the striatum in treating Parkinson’s disease, where focal intraparenchymal injections failed to deliver sufficient AAV in patients to achieve significant therapeutic effects [52,53]. By further refining ThUS parameters to maximize BBB opening volume per sonication, future studies can enhance the efficiency of gene delivery, improving the feasibility of noninvasive gene therapy applications for neurological disorders. Ongoing studies from our group are beginning to unravel additional effects of ThUS pulsing parameters on AAV delivery in a more granular fashion [54], while future studies will confirm the absence of adverse histopathological findings due to modified per-spot sonication parameters.

Given the ambitious objective to facilitate non-surgical, remote magnetogenetics, our study was not devoid of limitations. First, generally speaking, the low availability of experimental novel magnetogenetic actuators, namely reproducible batches of SPION and sufficient titers of AAV9-CaMKII-pTRPA1 precluded high-power replication of animal experiments. This also relates to a broader limitation imposed by the systemic route of injection and targeted ultrasound-mediated BBB opening. While improvements in ThUS pulse sequence design enabled increased gene delivery for a given systemic dose, scalable manufacturing techniques will be required for translation of non-invasive brain stimulation techniques and broader gene therapy applications to larger mammalian subjects, including humans. Nevertheless, without focal BBB permeabilization techniques like ThUS, negligible AAV expression and SPION deposition was observed within the brain, indicating a substantial improvement in magnetogenetic actuator delivery over conventional non-invasive delivery routes of administration such as IV injection alone.

The systemic administration approach also necessitates consideration of biodistribution profiles for both magnetogenetic components. For AAV-mediated overexpression of thermoreceptors and GEVI, we expect localized expression given the use of neuron-specific CaMKII promoters, where peripheral tissues should not exhibit substantial overexpression due to the inherent neuronal specificity of this promoter system. Regarding SPION biodistribution, the literature demonstrates that after systemic injection, SPIONs are primarily taken up by the reticuloendothelial system, with the highest concentrations observed in the liver and spleen, followed by the kidneys and bone marrow [55,56]. It has also been shown that tissue iron levels peak within 24 h post-injection and return to control or near-control levels within 7 days in most organs [57]. These studies have also found that SPIONs show increased iron levels in all organs tested except for the brain [57], suggesting limited brain penetration without BBB opening techniques such as those employed in our study. This further supports the rationale for using ThUS-mediated BBB opening to enhance SPION delivery to the brain for magnetogenetic applications. Future studies should systematically evaluate both SPION biodistribution in brain tissue following ThUS-mediated delivery and confirm the neuronal specificity of thermoreceptor/GEVI expression using the CaMKII promoter system across different organs to fully characterize the safety profile of this approach.

While engineered AAV capsids capable of crossing the BBB, such as AAV-PHP.eB, represent significant advancements in non-invasive brain-wide gene delivery in certain mouse strains, several critical limitations underscore the continued importance of FUS-mediated BBB opening for achieving therapeutically efficacious transgene expression levels. First, while engineered capsids demonstrate improved brain penetration, achieving therapeutically relevant expression levels across the entire brain often requires high systemic doses that pose significant safety risks. Recent clinical trials using high-dose systemic AAV administration have resulted in patient deaths, underscoring the continued need for dose-reduction strategies [58–60]. FUS-mediated BBB opening can synergistically enhance the brain penetration of both wild-type and engineered capsids, potentially enabling therapeutic efficacy at substantially lower systemic doses.

Second, the species translation challenge with engineered capsids remains a significant barrier to clinical implementation. While AAV-PHP.eB demonstrates excellent efficacy in certain mouse strains, its performance in primates when systemically administered is markedly reduced [61]. FUS-mediated delivery provides a capsid-agnostic enhancement strategy that can improve brain penetration regardless of the specific AAV variant employed. Even with optimally engineered capsids, previous studies have demonstrated that FUS can further increase the brain penetration of already BBB-crossing AAV variants, suggesting that combining these approaches may achieve superior therapeutic outcomes compared to either strategy alone. This synergistic enhancement is especially valuable given our observations that ThUS-facilitated delivery substantially improved magnetogenetic actuator delivery over conventional non-invasive routes such as IV injection alone, where negligible AAV expression and SPION deposition was observed within the brain.

Future studies will be required to assess and optimize each step in the initially-proposed closed-loop magnetogenetics technique. Optimization experiments should include harvesting brains from mice after varying levels of SPION delivery with ThUS-mediated BBB opening, followed by magnetic stimulation of brain sections with different systemic SPION concentrations to determine the dose threshold necessary for nanoparticle heating and subsequent pTRPA1 activation. Intraparenchymally injected SPIONs should serve as positive controls to establish baseline heating efficacy. Similarly, pTRPA1 overexpression levels must be systematically evaluated through in vivo behavioral magnetogenetic stimulation experiments, with intraparenchymally injected pTRPA1 AAV constructs serving as controls to define the minimum expression threshold required for reliable channel activation. Beyond uncovering these foundational dose-response relationships, future work must also

optimize the density of GEVIs required to accurately record neuronal spiking behavior mediated by pTRPA1 activation, ensuring sufficient signal-to-noise ratios for reliable closed-loop feedback control. These studies represent essential prerequisites for the advancement of non-invasive magnetogenetics approaches.

5. Conclusion

Technical improvements in brain stimulation techniques continue to enable discovery of underlying neuronal circuits relating to complex mammalian behavior. Beyond this, brain stimulation techniques have already proven useful in the context of therapy, perhaps most notably applied in Deep Brain Stimulation (DBS) as a breakthrough therapeutic for movement disorders including PD, essential tremor, and dystonia. However, the realization of non-invasive brain therapy with ThUS not only could provide patients with alternative options to surgery, but could also enable interrogation of complex neuronal pathways throughout the brain which is currently unachievable with highly focal and invasive gene delivery methods used in neuroscience research, including direct intraparenchymal injection.

CRediT authorship contribution statement

Alec J. Batts: Writing – review & editing, Writing – original draft, Visualization, Validation, Supervision, Software, Resources, Project administration, Methodology, Investigation, Funding acquisition, Formal analysis, Data curation, Conceptualization. **Fotios N. Tsitsos:** Investigation. **Jeannette Ingabire:** Writing – review & editing, Writing – original draft, Visualization, Methodology, Investigation, Conceptualization. **Guillaume Duret:** Writing – review & editing, Writing – original draft, Project administration, Conceptualization. **Samantha L. Gorman:** Visualization, Methodology, Investigation. **Deny Tsakri:** Visualization, Methodology, Investigation. **Rebecca L. Noel:** Methodology, Investigation. **Robin Ji:** Methodology. **Nancy Kwon:** Methodology, Investigation. **Quoc-Khanh Pham:** Investigation. **Linlin Zhang:** Investigation. **Gang Bao:** Project administration, Funding acquisition. **Jacob T. Robinson:** Supervision, Project administration, Funding acquisition, Conceptualization. **Elisa E. Konofagou:** Supervision, Project administration, Funding acquisition, Conceptualization, Editing - Original draft and revisions.

Data and materials availability

Data produced for this study can be made available upon reasonable request to the corresponding authors.

Funding

This study was funded in part by the National Institutes of Health grants R01EB009041, R01AG038961, R56AG038961 [EEK], the Naval Information Warfare Center (NIWC), the Cancer Prevention and Research Institute of Texas grant RP220518 [GB], and the Defense Advanced Research Projects Agency (DARPA) under Contract No. N66001-19-C-4020 [EEK, GB, JTR].

Declaration of competing interest

The authors declare the following financial interests/personal relationships which may be considered as potential competing interests: Elisa E. Konofagou reports financial support was provided by National Institutes of Health. Gang Bao, Jacob T. Robinson, & Elisa E. Konofagou reports financial support was provided by Defense Advanced Research Projects Agency. Gang Bao, PhD reports financial support was provided by Cancer Prevention and Research Institute of Texas. Elisa E. Konofagou reports a relationship with Delsona Therapeutics that includes: board membership. Jacob T. Robinson reports a relationship with Motif Neurotech that includes: employment. Elisa E. Konofagou has patent pending to Columbia University. Some of the methodology presented herein is supported by patents optioned to Delsona Therapeutics, Inc. where E.E.K. serves as co-founder and scientific adviser. The other authors declare that they have no known competing financial interests or personal relationships that could have appeared to influence the work reported in this paper.

Acknowledgements

The authors wish to thank Madhuvanthi Kannan, Ganesh Vasan, and Vincent A. Pieribone for expertise with GEVIs and for producing GEVI plasmids. The authors also wish to thank Xinghua Zeng at the University of North Carolina at Chapel Hill Vector Core, where AAV-GEVI constructs were synthesized, and Joshua Ortiz-Guzman and Ying Wang at the Baylor College of Medicine Optogenetics and Viral Vectors Core where AAV-pTRPA1 constructs were synthesized. The authors also wish to thank Daniel Hinojosa and Qingbo Zhang for assistance with SPION synthesis.

Appendix A. Supplementary data

Supplementary data to this article can be found online at https://doi.org/10.1016/j.brs.2025.10.006.

References

[1] Ji R, et al. Cavitation-modulated inflammatory response following focused ultrasound blood-brain barrier opening. J Contr Release 2021;337:458–71.
[2] Samiotaki G, Konofagou EE. Dependence of the reversibility of focused-ultrasound-induced blood–brain barrier opening on pressure and pulse length in vivo. IEEE Trans Ultrason Ferroelectrics Freq Control 2013;60:2257–65.
[3] Batts AJ, et al. Using a novel rapid alternating steering angles pulse sequence to evaluate the impact of theranostic ultrasound-mediated ultra-short pulse length on blood-brain barrier opening volume and closure, cavitation mapping, drug delivery feasibility, and safety. Theranostics 2023;13:1180–97.
[4] Batts AJ, Ji R, Kline-Schoder AR, Noel RL, Konofagou EE. Transcranial theranostic ultrasound for pre-planning and blood-brain barrier opening: a feasibility study using an imaging phased array in vitro and in vivo. IEEE Trans Biomed Eng 2022;69:1481–90.
[5] Choi JJ, et al. Microbubble-size dependence of focused ultrasound-induced blood-brain barrier opening in mice in vivo. IEEE Trans Biomed Eng 2010;57:145–54.
[6] Hynynen K, McDannold N, Vykhodtseva N, Jolesz FA. Noninvasive MR imaging–guided focal opening of the blood-brain barrier in rabbits. Radiology 2001;220:640–6.
[7] Noel RL, Gorman SL, Batts AJ, Konofagou EE. Getting ahead of Alzheimer's disease: early intervention with focused ultrasound. Front Neurosci 2023;17.
[8] Karakatsani ME, et al. Unilateral focused ultrasound-induced blood-brain barrier opening reduces phosphorylated tau from the rTg4510 mouse model. Theranostics 2019;9:5396–411.
[9] Kline-Schoder AR, et al. Characterization of the responses of brain macrophages to focused ultrasound-mediated blood–brain barrier opening. Nat Biomed Eng 2023:1–14. https://doi.org/10.1038/s41551-023-01107-0.
[10] Leinenga G, Götz J. Scanning ultrasound removes amyloid-β and restores memory in an Alzheimer's disease mouse model. Sci Transl Med 2015;7:278ra33.
[11] Karakatsani ME, et al. Focused ultrasound mitigates pathology and improves spatial memory in Alzheimer's mice and patients. Theranostics 2023;13:4102–20.
[12] Bae S, et al. Transcranial blood-brain barrier opening in Alzheimer's disease patients using a portable focused ultrasound system with real-time 2-D cavitation mapping. Theranostics 2024;14:4519–35.
[13] Rezai Ali R, et al. Ultrasound blood–brain barrier opening and aducanumab in alzheimer's disease. N Engl J Med 2024;390:55–62.
[14] Rezai AR, et al. Noninvasive hippocampal blood−brain barrier opening in Alzheimer's disease with focused ultrasound. Proc Natl Acad Sci 2020;117:9180–2.
[15] Mainprize T, et al. Blood-brain barrier opening in primary brain tumors with non-invasive MR-Guided focused ultrasound: a clinical safety and feasibility study. Sci Rep 2019;9:321.
[16] Englander ZK, et al. Focused ultrasound mediated blood–brain barrier opening is safe and feasible in a murine pontine glioma model. Sci Rep 2021;11:6521.
[17] Martinez P, et al. MRI-guided focused ultrasound blood–brain barrier opening increases drug delivery and efficacy in a diffuse midline glioma mouse model. Neuro-Oncol Adv 2023;5:vdad111.
[18] Sheybani ND, et al. Profiling of the immune landscape in murine glioblastoma following blood brain/tumor barrier disruption with MR image-guided focused ultrasound. J Neuro Oncol 2022;156:109–22.
[19] Sheybani ND, et al. ImmunoPET-informed sequence for focused ultrasound-targeted mCD47 blockade controls glioma. J Contr Release 2021;331:19–29.

[20] Blesa J, et al. BBB opening with focused ultrasound in nonhuman primates and Parkinson's disease patients: targeted AAV vector delivery and PET imaging. Sci Adv 2023;9:eadf4888.
[21] Mead BP, et al. Novel focused ultrasound gene therapy approach noninvasively restores dopaminergic neuron function in a rat parkinson's disease model. Nano Lett 2017;17:3533–42.
[22] Timbie KF, Mead BP, Price RJ. Drug and gene delivery across the blood-brain barrier with focused ultrasound. J Control Release Off J Control Release Soc 2015; 219:61–75.
[23] Wang F, et al. Targeted delivery of GDNF through the blood-brain barrier by MRI-guided focused ultrasound. PLoS One 2012;7:e52925.
[24] Samiotaki G, Acosta C, Wang S, Konofagou EE. Enhanced delivery and bioactivity of the neurturin neurotrophic factor through focused ultrasound-mediated blood–brain barrier opening in vivo. J Cereb Blood Flow Metab Off J Int Soc Cereb Blood Flow Metab 2015;35:611–22.
[25] Leung SA, et al. Transcranial focused ultrasound phase correction using the hybrid angular spectrum method. Sci Rep 2021;11:6532.
[26] Batts A, Konofagou E. Targeting accuracy of transcranial power cavitation imaging for blood-brain barrier opening using a theranostic phased array. In: 2020 IEEE International Ultrasonics Symposium (IUS); 2020. p. 1–3. https://doi.org/10.1109/IUS46767.2020.9251639.
[27] Batts A, Ji R, Noel R, Schoder AK, Konofagou E. The effect of pulse length on theranostic ultrasound-mediated blood-brain barrier opening volume, closing timeline, and cavitation mapping in vivo. In: 2021 IEEE International Ultrasonics Symposium (IUS); 2021. p. 1–3. https://doi.org/10.1109/IUS52206.2021.9593476.
[28] Ji R, Burgess M, Konofagou E. Transcranial blood-brain barrier opening and power cavitation imaging using a diagnostic imaging array. In: 2019 IEEE International Ultrasonics Symposium (IUS); 2019. p. 2–4. https://doi.org/10.1109/ULTSYM.2019.8926281.
[29] Ji R. Optimization of focused ultrasound mediated blood-brain barrier opening. New York, NY: Columbia University; 2021.
[30] Stanley SA, Friedman JM. Electromagnetic regulation of cell activity. Cold Spring Harb Perspect Med 2019;9:a034322.
[31] Sebesta C, et al. Subsecond multichannel magnetic control of select neural circuits in freely moving flies. Nat Mater 2022;21:951–8.
[32] Chen R, Romero G, Christiansen MG, Mohr A, Anikeeva P. Wireless magnetothermal deep brain stimulation. Science 2015;347:1477–80.
[33] Huang H, Delikanli S, Zeng H, Ferkey DM, Pralle A. Remote control of ion channels and neurons through magnetic-field heating of nanoparticles. Nat Nanotechnol 2010;5:602–6.
[34] Luo J, Shen WL, Montell C. TRPA1 mediates sensation of the rate of temperature change in Drosophila larvae. Nat Neurosci 2017;20:34–41.
[35] Gong Y, Wagner MJ, Li JZ, Schnitzer MJ. Imaging neural spiking in brain tissue using FRET-opsin protein voltage sensors. Nat Commun 2014;5:3674.
[36] Yang HH, St-Pierre F. Genetically encoded voltage indicators: opportunities and challenges. J Neurosci 2016;36:9977–89.
[37] Kannan M, et al. Dual-polarity voltage imaging of the concurrent dynamics of multiple neuron types. Science 2022;378:eabm8797.
[38] Hollidge BS, et al. Kinetics and durability of transgene expression after intrastriatal injection of AAV9 vectors. Front Neurol 2022;13:1051559.
[39] Fischell JM, Fishman PS. A multifaceted approach to optimizing AAV delivery to the brain for the treatment of neurodegenerative diseases. Front Neurosci 2021;15.
[40] Feshitan JA, Chen CC, Kwan JJ, Borden MA. Microbubble size isolation by differential centrifugation. J Colloid Interface Sci 2009;329:316–24.
[41] Wang S, Samiotaki G, Olumolade O, Feshitan JA, Konofagou EE. Microbubble type and distribution dependence of focused ultrasound-induced blood–brain barrier opening. Ultrasound Med Biol 2014;40:130–7.
[42] Hassan S, Ingabire J, Zhao X, Asfouri J, Robinson JT. Sensitive, accurate, and high spatiotemporal resolution photonic thermometry. Appl Phys Lett 2024;124: 211102.
[43] Kofoed RH, et al. Efficacy of gene delivery to the brain using AAV and ultrasound depends on serotypes and brain areas. J Control Release Off J Control Release Soc 2022;351:667–80.
[44] Burgess MT, Apostolakis I, Konofagou EE. Power cavitation-guided blood-brain barrier opening with focused ultrasound and microbubbles. Phys Med Biol 2018; 63:065009.
[45] Irrsack E, et al. Effects of local administration of iron oxide nanoparticles in the prefrontal cortex, striatum, and Hippocampus of rats. Neurotox Res 2021;39: 2056–71.
[46] Etheridge ML, et al. Accounting for biological aggregation in heating and imaging of magnetic nanoparticles. Technology 2014;2:214–28.
[47] Radhiyanti PT, Konno A, Matsuzaki Y, Hirai H. Comparative study of neuron-specific promoters in mouse brain transduced by intravenously administered AAV-PHP.eB. Neurosci Lett 2021;756:135956.
[48] Scheyltjens I, et al. Evaluation of the expression pattern of rAAV2/1, 2/5, 2/7, 2/8, and 2/9 serotypes with different promoters in the mouse visual cortex. J Comp Neurol 2015;523:2019–42.
[49] Fanselow MS, Dong H-W. Are the dorsal and ventral hippocampus functionally distinct structures? Neuron 2010;65:7.
[50] Moser MB, Moser EI, Forrest E, Andersen P, Morris RG. Spatial learning with a minislab in the dorsal hippocampus. Proc Natl Acad Sci USA 1995;92:9697–701.
[51] Pothuizen HHJ, Zhang W-N, Jongen-Rêlo AL, Feldon J, Yee BK. Dissociation of function between the dorsal and the ventral hippocampus in spatial learning abilities of the rat: a within-subject, within-task comparison of reference and working spatial memory. Eur J Neurosci 2004;19:705–12.
[52] Kordower JH. AAV2-Neurturin for parkinson's disease: what lessons have we learned? In: Manfredsson FP, editor. Gene therapy for neurological disorders: methods and protocols. New York, NY: Springer; 2016. p. 485–90. https://doi.org/10.1007/978-1-4939-3271-9_32.
[53] Bartus RT, et al. Bioactivity of AAV2-neurturin gene therapy (CERE-120): differences between Parkinson's disease and nonhuman primate brains. Mov Disord Off J Mov Disord Soc 2011;26:27–36.
[54] Tsitsos FN, Batts AJ, Jimenez DA, Macsemchuk CA, Li C, Ji R, Bae S, Ciaccio GL, Theodorou A, Ramirez RK, Gorman SL, Lugg CL, Konofagou EE. Characterization of microbubble cavitation in theranostic ultrasound-mediated blood-brain barrier opening for gene delivery. Journal of Controlled Release 2025;113986. https://doi.org/10.1016/J.JCONREL.2025.113986.
[55] Wahajuddin & Arora S. Superparamagnetic iron oxide nanoparticles: magnetic nanoplatforms as drug carriers. Int J Nanomed 2012;7:3445–71.
[56] Yu Q, et al. Biodistribution and toxicity assessment of superparamagnetic iron oxide nanoparticles in vitro and in vivo. Curr Med Sci 2018;38:1096–102.
[57] Pham BTT, et al. Biodistribution and clearance of stable superparamagnetic maghemite iron oxide nanoparticles in mice following intraperitoneal administration. Int J Mol Sci 2018;19:205.
[58] Lek A, et al. Death after high-dose rAAV9 gene therapy in a patient with Duchenne's muscular dystrophy. N Engl J Med 2023;389:1203–10.
[59] High-dose AAV gene therapy deaths. Nat Biotechnol 2020;38. 910–910.
[60] Philippidis A. Novartis confirms deaths of two patients treated with gene therapy zolgensma. Hum Gene Ther 2022;33:842–4.
[61] Liguore WA, et al. AAV-PHP.B administration results in a differential pattern of CNS biodistribution in non-human Primates compared with mice. Mol Ther 2019; 27:2018–37.